Upconverting nanovesicles for the activation of ruthenium anti-cancer prodrugs with red light

Askes, S.H.C.

CHAPTER 2

Introduction II: Light upconversion using triplet-triplet annihilation

Light upconversion is the conversion of low-energy light to high-energy light, which can be exploited in applications such as bio-imaging and photoactivated chemotherapy. Among the various principles of light upconversion, triplet-triplet annihilation upconversion (TTA-UC) holds great promise because it can be realized at low excitation intensities and with high efficiency. In this chapter, the TTA-UC mechanism is outlined in detail and nanoparticle systems are discussed with which TTA-UC can be achieved in biological systems. Furthermore, one of the fundamental issues of the TTA-UC mechanism is the inherent oxygen sensitivity. Because solving this issue is of critical importance for the advancement of biological TTA-UC applications, this chapter also discusses in detail how the oxygen sensitivity can be overcome in biological systems. Finally, an outline is given for this thesis.

Sven H.C. Askes and Sylvestre Bonnet. Manuscript in preparation

2.1 The principle of light upconversion

Light upconversion is the photophysical process in which light is converted from low energy (high wavelength, such as red light) to higher energy (low wavelength, such as blue light) by combining the energy of multiple photons. Light upconversion has been recognized to have great potential in biological applications such as bio-imaging and photoactivated chemotherapy (PACT). The advantages of upconversion bio-imaging are evident: first of all, *in vitro* upconversion bio-imaging with red to near-infrared excitation wavelengths reduces irradiation damage and allows a longer or more frequent observation. Secondly, because the emitted light has more energy than the excitation light, upconverted emission can be readily distinguished from autofluorescence so that an excellent imaging contrast can be achieved. Thirdly, red to near-infrared excitation light is able to penetrate deeper *in vivo* so that deeper imaging can be performed.

Besides bio-imaging, light upconversion can be used to activate PACT drugs, that are often only sensitive for UV to green light, with wavelengths in the phototherapeutic window (600 – 950 nm). This strategy is particularly suited for promising PACT drug classes such as blue-light sensitive ruthenium polypyridyl complexes (Chapter 1), Pt(IV) complexes that are activatable with UV to blue light,[1] light-cleavable organic moieties such as *o*-nitrobenzyl groups and coumarin derivatives that are activatable up to the green wavelength range,[2] and photo-isomerizing molecules such as azobenzenes.[3] Practically, this strategy involves red to near-infrared light being upconverted inside the tumor to blue light, which can then be used to activate a prodrug. Using red to near-infrared light instead of UV to green light would lead to a tumor treatment at greater tissue depth. Moreover, in contrast to UV to blue light, red to near-infrared light does not cause any tissue ablation at doses relevant to PACT (see Section 1.4).

The three most relevant forms of light upconversion in combination with PACT are two-photon absorption (TPA), lanthanoid-based upconverting nanoparticles (UCNPs), and triplet-triplet annihilation upconversion (TTA-UC). TPA relies on the simultaneous absorption of two low-energy photons by chromophores with high two-photon absorption cross sections, after which the combined energy of both photons can be used to trigger high-energy requiring photochemistry.[4] For example, this strategy has been explored with two-photon responsive Ru complexes[5] and for drug release from

photocleavable coumarin-derivatized vesicles.[6] Although appealing, the requirement that two photons must be simultaneously absorbed invokes the cumbersome and expensive use of high-power pulsed lasers. Moreover, the required high photon density (MW.cm^{-2} to GW.cm^{-2} irradiances)[7] are only obtained when the laser is focused to a microscopic irradiation volume. Obviously, treatment of a large tumor would be tedious and time-consuming. The alternative UCNPs are crystalline nano-sized particles that are made of low-phonon energy matrices, such as β-$NaYF_4$, that can be advantageously used as upconversion platform and drug carrier in one.[8] The upconverting properties rely on the sequential absorption of infrared photons (808 or 980 nm) by sensitizer lanthanoid ions such as Nd^{3+} or Yb^{3+} that transfer this energy multiple times to emitter ions such as Er^{3+}, Tm^{3+}, or Ho^{3+}.[8e] The combined energy is ultimately released in the form of UV, blue, green, and/or red photons.[8e] UCNPs are enormously popular for bio-imaging and drug activation purposes,[9] despite that they suffer from low quantum yields of upconversion (typically << 0.5% in aqueous solution), low absorbance coefficients, and the need for high power excitation (> 1 W.cm^{-2}) to achieve decent levels of prodrug activation.[10] Even in the NIR domain, high laser intensities (especially at 980 nm) leads to undesired tissue ablation.[11] In contrast, TTA-UC features much higher upconversion quantum yields (~5% in aqueous solution)[12] at much lower excitation intensities (typically < 0.2 W.cm^{-2}),[13] and features molecular chromophores with high molar absorption coefficients. Because of these advantages, the research described in this thesis explored the potential of combining TTA-UC and bio-imaging or PACT.

2.2 Triplet-triplet annihilation upconversion

TTA-UC was already demonstrated several times by Parker and Hatchard in the 1960s,[14] but in those days this phenomenon merely received recognition as photophysical curiosity. It was only in the 21st century that the principle was rediscovered and research on TTA-UC has since then received an exponentially growing amount of scientific interest.[15] Now, TTA-UC has become a powerful photophysical trick with promising applications such as oxygen sensing,[16] extending the action spectrum of photosynthetic organisms,[17] photocatalysis,[18] solar energy harvesting,[19] bio-imaging,[12, 20] and drug delivery and activation (*e.g.* PACT).[21]

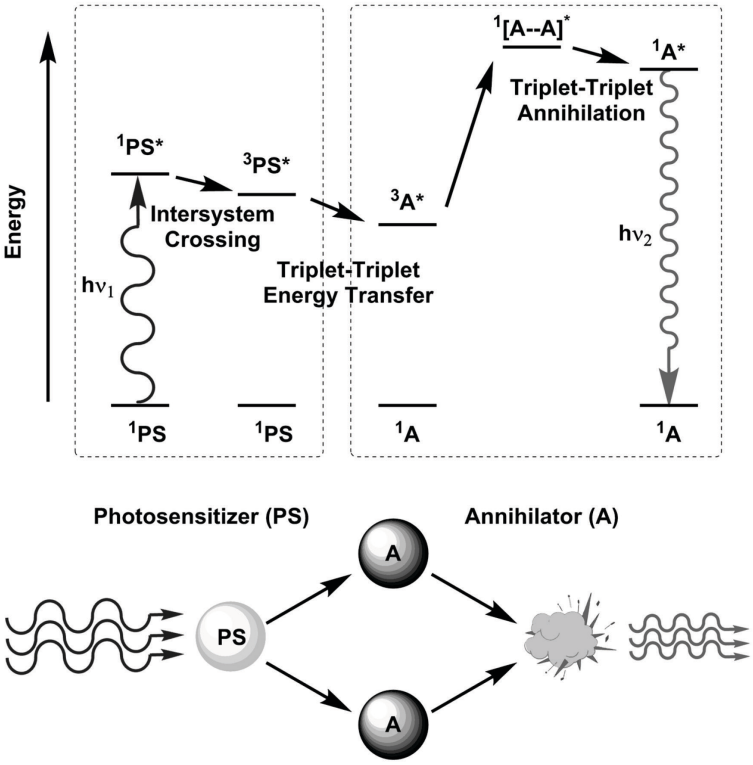

Figure 2.1. Jablonski diagram of the photophysical processes involved in TTA-UC.

TTA-UC is based on the photophysical interplay of photosensitizer (**PS**) and annihilator chromophores (**A**), see Figure 2.1.[4, 9f, 15a, 22] The photosensitizer absorbs low energy light ($h\nu_1$), after which intersystem crossing (ISC) leads to a long-lived triplet state (Equation 2.1):

$$^1\boldsymbol{PS} + h\nu_1 \xrightarrow{r_{abs}} {}^1\boldsymbol{PS}^* \xrightarrow{k_{ISC}} {}^3\boldsymbol{PS}^* \qquad \textit{Equation 2.1}$$

where r_{abs} is the rate of light absorption by the photosensitizer (in mol.L^{-1}.s^{-1}), and k_{ISC} is the rate constant of ISC (in s^{-1}). The triplet state energy of ^{3}**PS*** is transferred to the annihilator by a Dexter-type energy transfer upon diffusional collision, called triplet-triplet energy transfer (TTET); a succession of TTET leads to a buildup of triplet state annihilator molecules due to a generally very long triplet state annihilator lifetime (Equation 2.2):

$$^3\boldsymbol{PS}^* + {}^1\boldsymbol{A} \xrightarrow{k_{TTET}} {}^1\boldsymbol{PS} + {}^3\boldsymbol{A}^* \qquad \textit{Equation 2.2}$$

where k_{TTET} is the second-order rate constant of TTET (in $M^{-1}.s^{-1}$). At this stage, triplet back transfer from annihilator to sensitizer is usually eliminated by keeping the sensitizer to annihilator molar ratio very low (typically 1:10 to 1:200).[23] Then, two excited state triplet annihilator molecules produce an encounter-pair upon diffusional collision. The encounter-pair has either singlet, triplet, or quintet multiplicity, with 1/9, 3/9, and 5/9 chance of formation, respectively (discussed in more detail later). The singlet-state encounter-pair will result in triplet-triplet annihilation (TTA), where one molecule departs in a higher-energy singlet excited state while the other converts to the ground state (Equation 2.3):

$$^3\boldsymbol{A}^* + {}^3\boldsymbol{A}^* \rightarrow {}^1(\boldsymbol{A}-\boldsymbol{A})^* \rightarrow {}^1\boldsymbol{A}^* + {}^1\boldsymbol{A} \qquad \textit{Equation 2.3}$$

where this overall TTA step is a bimolecular process and thus has a second-order rate constant, k_{TTA} (in $M^{-1}.s^{-1}$). Note that TTA is only possible if the energy of the encounter pair exceeds the energy of the singlet excited annihilator. Finally, the singlet excited state returns to the ground state by fluorescent emission of a high energy photon ($h\nu_2$), realizing light upconversion (Equation 2.4):

$$^1\boldsymbol{A}^* \xrightarrow{k_F} {}^1\boldsymbol{A} + h\nu_2 \qquad \textit{Equation 2.4}$$

where k_F is the rate constant of annihilator fluorescence (in s^{-1}). Due to the dependence on molecular contact in the TTET and TTA steps, the overall process heavily relies on the diffusion of sensitizer and/or annihilator chromophores. In case molecular diffusion is restricted, it may rely on diffusion of the triplet excitons through the material.[23] In systems that rely on molecular diffusion, it is often found that the TTA step is rate-limiting, *i.e.* the TTA-rate has values comparable to the rate of molecular diffusion.[23] In such systems, the TTA-UC mechanism is therefore very dependent on the viscosity of the host material or solution.[15a, 23-24]

The anti-stokes shift, *i.e.* the wavelength difference between excitation source and the lowest emission maximum, determines the maximum upconversion energy gain of TTA-UC (ΔE_{UC}, in eV) that can be achieved. ΔE_{UC} is limited to twice the energy of the incident photon, because TTA-UC is a two-photon process. However, this limit is in practice never reached, because of inevitable enthalpic energy losses during ISC (ΔH_1 in eV), TTET (ΔH_2 in eV), and TTA (ΔH_3 in eV). ΔE_{UC} is therefore constrained by the sum of enthalpic losses, as described by Equation 2.5:[25]

$$\Delta E_{UC} = 2(h\nu_1 - \Delta H_1 - \Delta H_2) - \Delta H_3 \qquad \textit{Equation 2.5}$$

where $h\upsilon_1$ is the energy of the absorbed photons (in eV). Of these energy losses, ΔH_2 is most easily reduced by carefully aligning sensitizer and annihilator excited state triplet levels. The highest ΔE_{UC} thus far achieved is 0.94 eV for a couple that is excited at 670 nm ($h\upsilon_1$ = 1.85 eV) and emits at 445 nm ($h\upsilon_2$ = 2.79 eV). [25]

The evolutions in time of the excited states in the TTA-UC scheme are governed by the following set of rate equations (Equation 2.6 to Equation 2.9):

$$\frac{d[^1\boldsymbol{PS}^*]}{dt} = r_{abs} = \frac{\varphi_{exc}\left(1 - 10^{-A_{\lambda_{exc}}}\right)}{V} \qquad \textit{Equation 2.6}$$

$$\frac{d[^3\boldsymbol{PS}^*]}{dt} = k_{ISC}[^1\boldsymbol{PS}^*] - k_p[^3\boldsymbol{PS}^*] - k_{^3PS}[^3\boldsymbol{PS}^*] - k_{TTET}[^3\boldsymbol{PS}^*][^1\boldsymbol{A}] \qquad \textit{Equation 2.7}$$

$$\frac{d[^3\boldsymbol{A}^*]}{dt} = k_{TTET}[^3\boldsymbol{PS}^*][^1\boldsymbol{A}] - k_{^3A}[^3\boldsymbol{A}^*] - k_{TTA}[^3\boldsymbol{A}^*]^2 \qquad \textit{Equation 2.8}$$

$$\frac{d[^1\boldsymbol{A}^*]}{dt} = k_{TTA}[^3\boldsymbol{A}^*]^2 - k_F[^1\boldsymbol{A}^*] - k_{^1A}[^1\boldsymbol{A}^*] \qquad \textit{Equation 2.9}$$

where φ_{exc} is the photon flux at the excitation wavelength (mol photons.s^{-1}), $A_{\lambda_{exc}}$ is the absorbance at the excitation wavelength (assuming only **PS** absorbs at this wavelength), V is the irradiation volume (in L), k_p is the rate

constant of sensitizer phosphorescence (in s^{-1}), $k_{^3PS}$ is the non-radiative decay rate constant of ^{3}**PS*** (in s^{-1}), $k_{^3A}$ is the decay rate constant of ^{3}**A*** when no TTA occurs (in s^{-1}; usually only non-radiative decay), , and $k_{^1A}$ is the non-radiative decay rate constant of $^1\boldsymbol{A}^*$. Finally, note that the set of rate equations listed above described a rather simplified TTA-UC scheme: it does not account for (i) triplet back-transfer from ^{3}**A*** to ^{1}**PS**, (ii) hetero TTA between ^{3}**PS*** and ^{3}**A***, and (iii) homo TTA between pairs of ^{3}**PS***, which may become relevant at high [**PS**] and high excitation intensity.[7b, 22]

From Equation 2.6 to Equation 2.9, the overall efficiency of TTA-UC (Φ_{UC}) under stead-state conditions, defined as the number of upconverted photons per number of excited state photosensitizers upon illumination, is expressed by Equation 2.10:[23]

$$\Phi_{UC} = \frac{number\ of\ upconverted\ photons}{number\ of\ excited\ state\ PS} = \frac{1}{2}\Phi_{ISC}\Phi_{TTET}\Phi_{TTA}\Phi_F \qquad \textit{Equation 2.10}$$

in which Φ_{ISC} is the quantum yield of intersystem crossing, Φ_{TTET} the quantum yield of TTET, Φ_{TTA} the quantum yield of triplet-triplet annihilation, and Φ_F the quantum yield of fluorescence of the annihilator. The factor ½ accounts for the fact that two excited state photosensitizers maximally produce one excited singlet-state annihilator, *i.e.* the intrinsic maximum Φ_{UC} is 50%. Overall, Equation 2.10 underlines that each step needs to be optimized for a high Φ_{UC}. Usually, **PS** and **A** are chosen so that Φ_{ISC} and Φ_F have values close to unity, and k_{ISC} and k_F are generally very fast and thus not rate-limiting. Therefore, the overall efficiency is mainly governed by Φ_{TTET} and Φ_{TTA}. In the steady state (continuous wave excitation) Φ_{TTET} is expressed as the ratio of the quenching rate of ^{3}**PS*** ($k_{TTET}[^1\mathbf{A}][^3\mathbf{PS}^*]$, in $mol.L^{-1}.s^{-1}$) and the total decay rate of ^{3}**PS*** in presence of annihilator (Equation 2.11):[22]

$$\Phi_{TTET} = \frac{k_{TTET}[^1\boldsymbol{A}][^3\boldsymbol{PS}^*]}{k_p[^3\boldsymbol{PS}^*] + k_{^3PS}[^3\boldsymbol{PS}^*] + k_{TTET}[^1\boldsymbol{A}][^3\boldsymbol{PS}^*]} = \frac{k_{TTET}[^1\boldsymbol{A}]}{k_p + k_{^3PS} + k_{TTET}[^1\boldsymbol{A}]} \qquad \textit{Equation 2.11}$$

This expression states that higher annihilator concentrations lead to higher TTET efficiencies. For example, for a TTA-UC system in organic solution with a **PS** lifetime of 300 µs (*i.e.* $k_p + k_{^3PS} = 3 \times 10^4$ s^{-1}), 10 mM **A**, and realizing that triplet energy transfer in solution is usually diffusion limited (*i.e.* $k_{TTET} \approx 1 \times 10^9$ M^{-1}.s^{-1}),[22] the triplet quenching rate has a value of 10^7 s^{-1} and thus near unity energy transfer efficiencies are obtained. Next, Φ_{TTA} can be expressed in the steady state (continuous wave excitation) as the ratio of the triplet-triplet annihilation rate ($k_{TTA}[^3\mathbf{A}^*]^2$, in mol.L^{-1}.s^{-1}) and the total decay rate of the annihilator triplets (Equation 2.12):[22]

$$\Phi_{TTA} = f \times \frac{k_{TTA}[^3\boldsymbol{A}^*]^2}{k_{^3A}[^3\boldsymbol{A}^*] + k_{TTA}[^3\boldsymbol{A}^*]^2} = f \times \frac{k_{TTA}[^3\boldsymbol{A}^*]}{k_{^3A} + k_{TTA}[^3\boldsymbol{A}^*]} \qquad \textit{Equation 2.12}$$

where f is the spin statistical factor. This factor f takes into account that the encounter-pair of the two triplet state annihilator molecules has either singlet, triplet, or quintet multiplicity, with 1/9, 3/9, or 5/9 probability, respectively; only the singlet state multiplicity leads to the desired high-energy excited singlet state. However, because quintet states are not energetically accessible and triplet state encounter-pairs are partially recycled into triplet excited state annihilator molecules, the probability can be increased to 40% (i.e. f = 0.4).[15a, 23, 26] In some systems, f can be even further increased to approach unity.[7b] Furthermore, Equation 2.12 underlines that the TTA efficiency is directly dependent on the production of $^3\mathbf{A}^*$ and approaches unity when $k_{^3A} << k_{TTA}[^3\mathbf{A}^*]$, also known as the "strong annihilation regime". Usually, annihilators are chosen with metastable triplet states that feature lifetimes in the millisecond range (*i.e.* $k_{^3A} \approx 1 \times 10^3$).[22, 27] For instance, at a diffusion-limited TTA rate (*i.e.* $k_{TTA} \approx 1 \times 10^9$ M^{-1}.s^{-1}) this means that a triplet concentration of about 1×10^{-6} M would lead to a 50% TTA efficiency. Furthermore, it is important to realize that in the strong annihilation regime, Φ_{TTA} becomes a constant and the overall TTA-UC process becomes only dependent on the rate of triplet production, *i.e.* light absorption, as described in more detail in recent kinetic treatments.[26] In other words: in the strong annihilation regime, the triplet state manifold is so well-populated that TTA is the predominant photophysical route and competing quenching processes are negligible.[23, 26c] This has the immediate consequence that in the "weak annihilation regime" (*i.e.* when $k_{^3A} >> k_{TTA}[^3\mathbf{A}^*]$) , the intensity variation of TTA-UC is quadratically dependent on the excitation intensity variation – as

would be expected for a two-photon process –, while in the strong annihilation regime this dependence becomes linear. Indeed, this phenomenon is systematically observed for TTA-UC systems, see Figure 2.2. The transition point at which this excitation intensity dependency shifts from quadratic to linear is called the intensity threshold (I_{th}), and is strictly defined as the intensity at which the value of Φ_{UC} is half of the maximum.[7b] Monguzzi *et al.* have demonstrated that the value of I_{th} is proportional to $(k_{3_A})^2$ and is inversely proportional to k_{TTA}, Φ_{TTET}, and $A_{\lambda_{exc}}$.[7b] Thus, in order to obtain high Φ_{UC} at low excitation intensity, (i) annihilators with long lived triplet states are required, (ii) the absorbance of **PS** needs to be high (due to high [**PS**], high molar extinction coefficient, or both), (iii) the TTET step should occur with near-unity yield, and (iv) the TTA rate should be maximized. Typically, I_{th} has a value below 0.2 W.cm^{-2}, while the lowest reported value thus far is 6 μW.cm^{-2}.[28] To put these values in perspective, the solar radiance at the earth surface (AM1.5) is about 0.1 W.cm^{-2} and the linear power regime for lanthanoid-based upconverting nanoparticles is only reached at excitation intensities above 150 W.cm^{-2}.[10]

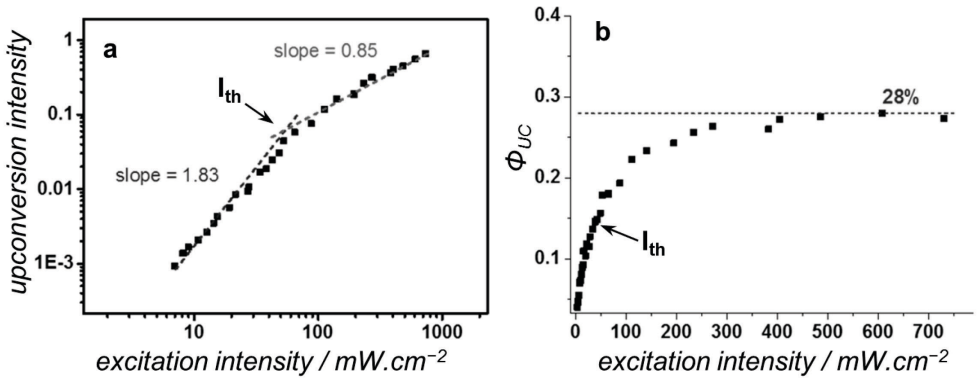

Figure 2.2. Typical power dependency of upconversion emission in a TTA-UC scheme. As an example, data of a green-to-blue upconverting system is shown with an I_{th} of 0.05 W.cm^{-2} and a maximum Φ_{UC} of 28%. (a) Upconversion emission intensity as a function of excitation intensity. The indicated slopes are obtained when the data is plotted on a double logarithmic scale. (b) Upconversion quantum yield (Φ_{UC}) as a function of excitation intensity. Reprinted (adapted) with permission from Duan et al.[29] © American Chemical Society.

The combined photophysical properties of photosensitizer and annihilator greatly influence Φ_{UC} and ΔE_{UC}, and only well-chosen combinations of photosensitizer and annihilator will lead to TTA-UC. The most important requirement for TTA-UC is the energy match between the triplet state energy levels of both molecules: ideally, the triplet energy level of the annihilator is

slightly lower in energy than the triplet energy level of the photosensitizer to accommodate favorable TTET. Besides this, the desirable characteristics of the photosensitizer include (i) high molar extinction coefficient, (ii) high ISC efficiency (Φ_{ISC}), (iii) long triplet lifetime (τ_T), and (iv) small singlet-triplet energy gap.[15a, 23, 30] These criteria are very well satisfied by palladium or platinum porphyrin complexes, which therefore have become benchmark photosensitizers in TTA-UC schemes. Typical examples are palladium tetra-(di-*tert*-butyl)phenyltetraquinoxalino porphyrin (PdTPTQP), palladium tetraphenyltetrabenzoporphyrin (PdTPTBP), and platinum octaethylporphyrin (PtOEP), see Figure 2.3. Moreover, metalloporphyrins usually feature a large absorption gap between Q-bands and Soret bands, so that re-absorption of the upconverted light is mostly eliminated. For the annihilator the most important requirements are (i) high fluorescence quantum yield (Φ_F), (ii) long triplet lifetime (τ_T), (iii) an excited singlet state with slightly less than twice the energy of the excited triplet state, and (iv) an excited singlet state with higher energy than the wavelength used to excite the photosensitizer.[15a, 23] Suitable annihilator molecules include anthracene, pyrene, perylene, rubrene, and diphenyl anthracene (DPA), see Figure 2.3.

A few early examples of well-matching photosensitizer-annihilator combinations are given in Table 2.1; numerous other examples have been reviewed elsewhere.[4, 9f, 15a] All of these sensitizer-annihilator pairs exhibit very large anti-stokes shift from green/red to blue (0.72-0.94 eV shift), and their relevant energy levels satisfy the requirements discussed earlier. It is worthwhile to note that these early results have been acquired in deoxygenated apolar organic solvents to dissolve the highly lipophilic molecules and to prevent quenching by molecular oxygen, which is the most predominant quenching pathway in TTA-UC schemes. Since these early examples in organic solution, TTA-UC has been demonstrated in rubbery and glassy polymers,[15a, 23-24, 31] hydro-, organo- and ionogels,[32] and a variety of nano- and micro-sized particle systems.[12-13, 18b, 20, 28, 33]

Table 2.1: Examples of photosensitizer-annihilator combination and their main TTA-UC properties.

Photosensitizer	**Annihilator**	λ_{exc} **(nm)**	λ_{em} **(nm)**	ΔE_{UC} **(eV)**	Φ_{UC} **(%)**	**Ref.**
PdTPTQP	perylene	670	445	0.94	0.6	[25]
PdTPTBP	3-(4-tert-butylphenyl)perylene	635	450	0.81	6.6	[34]
PtOEP	DPA	536	410	0.72	19	[35]
$[Ru(dmbpy)_3]^{2+}$ [a]	anthracene	514.5	375	0.90	-	[36]

[a] dmbpy = 4,4′-dimethyl-2,2′-bipyridine

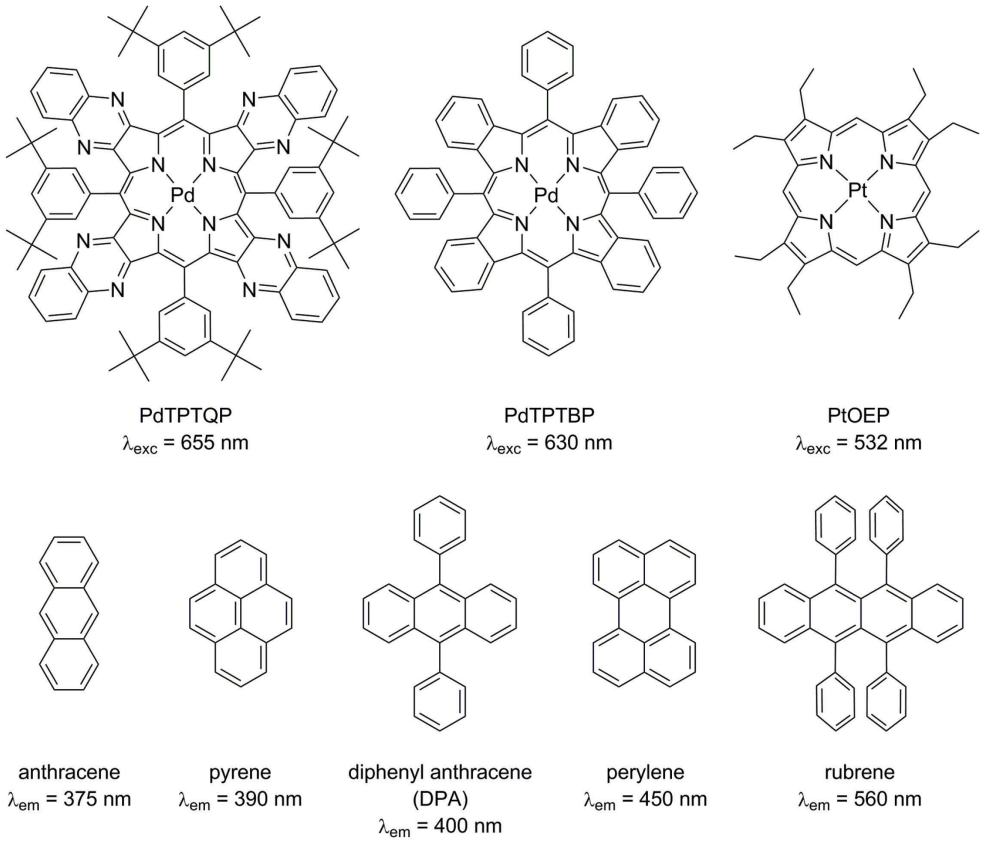

Figure 2.3. Chemical structures of frequently-used photosensitizers (top row) and annihilators (bottom row) in TTA-UC schemes. Approximate values for the highest absorption bands of photosensitizers and lowest emission peaks of annihilators are mentioned.[15a, 25]

2.3 Overcoming the oxygen sensitivity of TTA-UC

Whereas for some applications the oxygen sensitivity of TTA-UC can be exploited, for example to build an oxygen sensor,[16] for most other applications oxygen quenching leads to dysfunctional systems in which (i) upconversion does not work in air, and (ii) the highly reactive singlet oxygen that is generated by this quenching process leads to photodamage of the chromophores and the matrix (Figure 2.4). To counter these issues, several approaches have been developed in recent years. First of all, it has been shown that TTA-UC systems with very high TTET and TTA rates are less sensitive, because upconversion then successfully competes with the diffusion of oxygen. Especially promising are systems that feature supramolecular annihilator networks that support facile migration of triplet excitons. For example, the work of Kimizuka and coworkers shows that organogels or nano-

MOFs are excellent host systems for TTA-UC: densely-packed annihilator networks resulted in triplet exciton diffusion rates that by far exceed the molecular diffusion rate of molecules in organic solvents.[28-29, 32b, 32c, 37] The second strategy involves using matrices that obstruct the diffusion of molecular oxygen, which has been exemplified with polymers that were covalently or non-covalently functionalized with sensitizer and annihilator.[31b, 31h, 31i, 38] However, the low diffusion rate in these materials generally caused the upconversion efficiency to be low. An interesting solution to this problem was presented by Baluschev and Landfester *et al.*, who encapsulated micron-sized red-to-green upconverting oil-core nanocapsules in a cellulose matrix.[39] The cellulose acted as an oxygen barrier, so that TTA-UC was allowed to be efficient (Φ_{UC} = 4.1%) and long lasting in air. In other work by the same authors in collaboration with Turshatov, similar nanocapsules of 100 – 140 nm in diameter were embedded in electrospun polyvinyl alcohol (PVA) nanofibers with a diameter of 270 – 480 nm.[40] This nm-thick PVA wrapping successfully blocked diffusion of oxygen to the nanocapsules. These results show that it is possible to block oxygen with a nm-scale coating of an oxygen impermeable material.

Finally, it has been realized that oxygen sensitivity can be eliminated by the use of (singlet) oxygen scavengers. The idea of ground-state oxygen scavenging is self-evident: a reducing agent is added to remove dissolved oxygen so that the solution is deoxygenated until depletion of the scavenger. For instance, sodium sulfite has been used to deoxygenate a green-to-blue upconverting oil-in-water micro-emulsion.[33i] In the case of singlet oxygen scavenging, oxygen is consumed only upon irradiation of the sensitizer (Figure 2.4). Upon irradiation, singlet oxygen is produced which then reacts with the scavenger, causing a locally deoxygenated environment around the photosensitizer (micro-)environment. Once the oxygen concentration is low enough, TTA-UC is no longer restricted and upconverted light effectively appears upon further irradiation. Suitable scavengers that have been used for TTA-UC are alkene-terminated polyisobutylene, oleic acid, linoleic acid, and hyper-branched unsaturated polyphosphates.[12b, 12c, 13a, 31e, 33b, 33f] The former three examples rely on the reaction of the unsaturated bond with singlet oxygen to make peroxide derivatives.

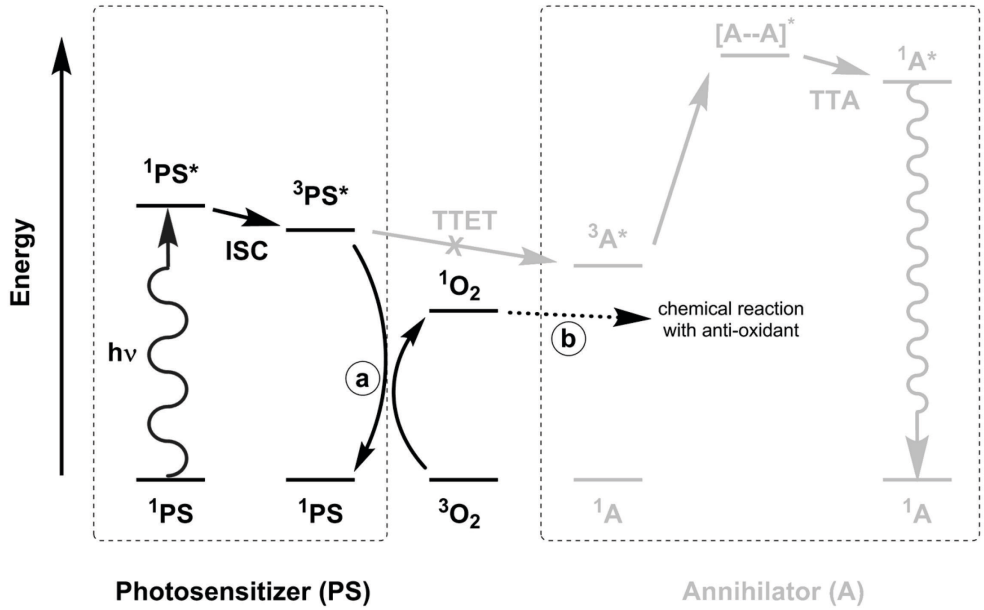

Figure 2.4. Oxygen sensitivity of the TTA-UC mechanism: After the photosensitizer reaches the triplet excited state, instead of engaging in triplet-triplet energy transfer (TTET) to the annihilator, it is quenched by ground state molecular oxygen to produce singlet oxygen (a). Quenching of the triplet state annihilator by oxygen can also occur (not shown). To overcome this issue, sacrificial anti-oxidants can be added to the mixture which chemically react with singlet oxygen (b). Then, TTA-UC is no longer restricted when the oxygen concentration is (nearly) depleted.

With biological TTA-UC applications in mind, quenching by molecular oxygen is also an especially important issue. For instance, using an oxygen-sensitive device for tumor imaging or treatment would surely lead to unreliable results, because oxygen concentrations vary drastically in the complex microenvironment of a tumor.[41] In the remaining sections of this chapter TTA-UC nanoparticles are described that have been used in bio-imaging or for PACT, and strategies to reduce the *in vitro* oxygen sensitivity are discussed.

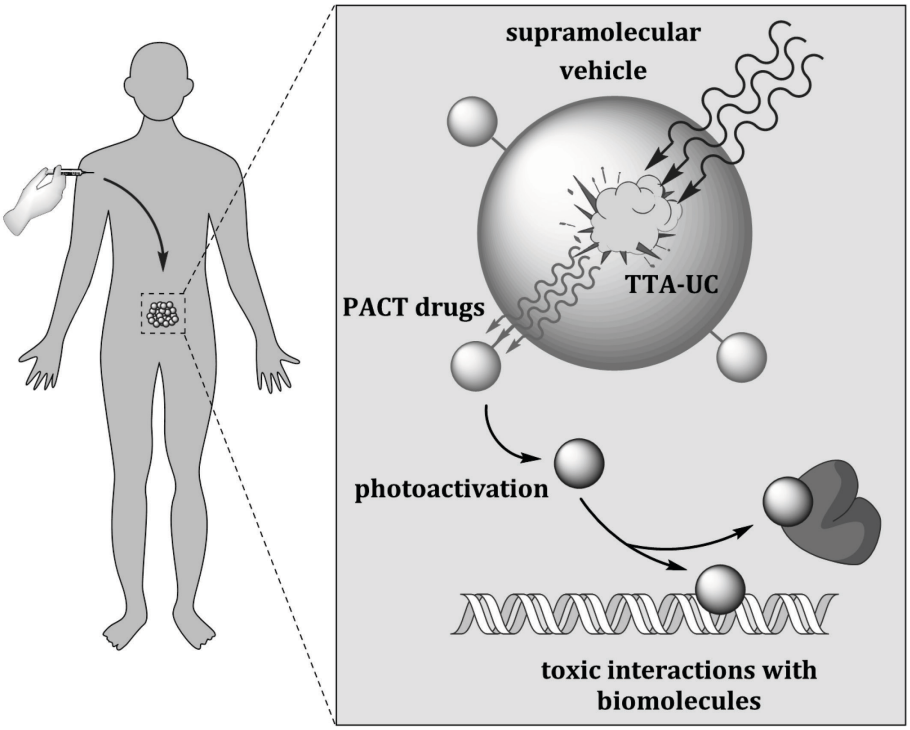

Figure 2.5. Schematic representation of the combination of a supramolecular vehicle, TTA-UC, and PACT drugs for in vivo tumor treatment. The device is injected in the body, after which it accumulates at the tumor site and the tumor is irradiated with red light. The red light is then locally upconverted to blue light, which activates the PACT prodrug (blue) anchored to the vehicle's surface or kept inside the vehicle. After irradiation the activated drug (red) dissociates from the vehicle and causes toxic interactions with biomolecules.

2.4 TTA-UC in bio-imaging and PACT

For biological TTA-UC applications, it is essential to combine sensitizer and annihilator in a supramolecular manner, so that they colocalize at the required site, and to facilitate molecular contact and migration of triplet states. Additionally, for PACT it is highly desirable to compartmentalize the light-activatable prodrug together with the upconversion dye-pair, in order to utilize the upconverted light effectively (Figure 2.5). Meanwhile, supramolecular vehicles such as nanoparticles have emerged as extremely versatile tools in biomedical applications.[2, 42] Because the TTA-UC dye pairs are usually very lipophilic, supramolecular systems are preferred with very lipophilic compartments. So far, six systems have emerged in which water-soluble nano-systems are combined with TTA-UC in a biological setting: silica-coated Pluronic F127 micelles,[12a, 20b] polylactic acid-block-polyethylene glycol

(PLA-b-PEG) micelles,[33j] dye-modified cellulose templates,[20c] and a variety of oil-core nanocapsules,[12b, 12c, 20a, 20d] see Table 2.2. These systems will be further detailed in this section. Furthermore, in Chapter 8 and Chapter 9 we report the imaging of upconversion luminescence in cancer cells using liposomes and polymersomes as carrier systems.

Green-to-blue upconverting silica-coated Pluronic F127 micelles were prepared in the group of Li.[12a] It was demonstrated that these micelles were non-toxic, had a high upconversion quantum yield, and could be used for *in vitro* upconversion imaging of cells and *in vivo* upconversion imaging of mouse lymph nodes. In a later publication,[12b] it was reported that particles created with this experimental procedure, but functionalized with a red-to-green or red-to-yellow upconverting pair instead only resulted in very weak upconversion emission. In a similar strategy, polylactic acid-block-polyethylene glycol was used to self-assemble green-to-blue upconverting micelles.[33j] The authors hypothesized that the upconverted blue emission was transferred *via* FRET to a blue-light responsive coumarin derivative, which induced photo-uncaging of a cell-binding peptide. However, control experiments in which the annihilator or sensitizer was omitted from the micelle formulation were not considered, so that it cannot be confirmed that uncaging of the peptide was indeed caused by TTA-UC. Regardless, after irradiation *ex vivo* with green light, and adding the nanoparticle suspension to cells, the nanoparticles showed a large increase in cell-binding. The functioning of this strategy in more biologically relevant conditions has yet to be demonstrated. The group of Siegwart prepared 350 nm sized cellulose aggregates that were functionalized with an infrared-to-yellow upconverting TTA-UC pair.[20c] The aggregates were taken up by HeLa cells in 2D culture and after intratumoral injection in a xenograft mouse model. The topics of oxygen sensitivity, upconversion efficiency, particle morphology, and biocompatibility of the approach were unfortunately not addressed.

Four types of oil-core nanocapsules with average hydrodynamic sizes from 100 - 200 nm have been demonstrated to be excellent hosts for TTA-UC, and were successfully imaged *in vitro* and *in vivo*.[12b, 12c, 20a, 20d] The oily interior favors molecular diffusion and effectively dissolves large amounts of hydrophobic compounds in a small particle volume. The exact chemical composition of both core and shell greatly affected the upconverting capabilities of the particles in presence of oxygen. First of all, the group of Landfester and Turshatov demonstrated green-to-blue upconversion with

hexadecane-core PSAA-shell (PSAA = polystyrene-polyacrylic acid copolymer) nanocapsules.[20d] These particles only produced upconversion after deoxygenation, and only "*in vitro"* after fixation and sealing of the sample in a glove box. In a next paper, red-to-green upconverting 1-phenylhexadecane-core PMMA-shell (PMMA = polymethyl methacrylate) were reported.[20a] Likewise, no upconversion in air could be established, which suggests that a nano-scale polymeric shell cannot safeguard the dyes inside the particles from quenching by oxygen. However, in living HeLa cells, some upconversion emission was in fact observed. Interestingly, upconversion brightened when the cells were treated with valinomycin, which stimulates mitochondria to enhance their oxygen consumption. This example demonstrates that *ex vitro* air stability is no definite prerequisite for obtaining upconversion *in vitro*. It is unclear why TTA-UC systems that do not work in air are capable of upconversion in living cells. We speculate that the presence of endogenous anti-oxidants are responsible for scavenging ground-state or singlet oxygen (see Section 2.3). Differences in oxygen concentration within each cell and differences between cells may also modify the ability of particles to perform TTA-UC.

The group of Li prepared red-to-green and red-to-yellow upconverting soy bean oil-core BSA-dextran-shell nanocapsules (BSA = bovine serum albumin).[12b] This system was able to perform upconversion in air. It was for the first time realized that reductive compounds can facilitate TTA-UC: soy bean oil contains oleic acid and linoleic acid, which both are unsaturated fatty acids that react with singlet oxygen, see Section 2.3. As mentioned before, the underlying rationale is that in an oxygen-rich environment, the photosensitizer produces singlet oxygen that can react with a scavenger, resulting in a locally deoxygenated micro-environment. Apart from the "reducing oil core", it was proposed that the BSA-shell participated in singlet oxygen scavenging, because BSA contains many tryptophan residues that are capable of reacting with singlet oxygen as well. Although the performance of the particles in 2D cell cultures was not established, the particles were successfully used for lymphatic imaging of living mice. Finally, the group of Kim prepared red-to-blue and red-to-green upconverting oleic acid-core silica shell nanocapsules.[12c] Here, pure oleic acid was chosen as scavenger to allow the particles to upconvert in air. From the article, it was not clear whether the particles were functional in 2D cell cultures, as the data showed fixated cells to which a commercial anti-fading reagent was added. Regardless, the particles

were successfully used in imaging of tumors *in vivo* with upconversion luminescence. Overall, from reviewing these published TTA-UC particle systems, it becomes clear that acquiring upconversion *in vitro* and *in vivo* has been a poorly explored subject so far.

2.5 Emission stability of TTA-UC in a biological context

A poorly addressed research topic is the emission stability in time of TTA-UC nanoparticles in a biological context. To the best of our knowledge, the emission stability has only been briefly discussed in the work of Li *et al.*, who show that green-to-blue upconversion of silica-coated Pluronic F127 micelles in HeLa cells was completely stable for at least 10 minutes under continuous illumination (no exact excitation intensity given);[12a, 20b] no further explanation is given why the emission is so stable. Of course, the stability requirements depend greatly on the application. Long-term bio-imaging methods require stable emission for seconds to minutes under continuous irradiation, but for short-term experiments, the emission stability is not especially critical. For the combination of TTA-UC and PACT, high stabilities are required up to hours of irradiation time at high irradiances (up to ~1 $W.cm^{-2}$) in order to release enough biologically active species. For instance, in comparable work that combines lanthanoid-based upconverting nanoparticles and PACT/PDT, typical treatment durations vary from 20 min up to more than 5 h.[43] Two critical questions are therefore: (i) how long-lasting is the upconversion emission in a biological context with current nanoparticle systems and (ii) how can the emission stability be improved? For instance, as mentioned before, many TTA-UC nanoparticles rely on the presence of endogenous or supplemental anti-oxidants in order to function *in vitro* or *in vivo*. However, after a certain time, the anti-oxidants may be depleted and oxygen can quench the TTA-UC process once again. Overall, the temporal stability of TTA-UC emission in a biological context, and the enhancement of this stability with for example anti-oxidants, are important aspects that need to be considered in future work. We argue that it is simply not enough to only demonstrate that a given TTA-UC system functions in air-equilibrated solutions: it is of utmost importance to show the temporal stability at a given excitation intensity and a given oxygenation level in order to conclude on the usability of a system for each specific application.

Table 2.2. Summary of known TTA-UC nanoparticle systems that have been developed for bio-imaging and PACT purposes, and their most important (photo)physical properties.

	Vesicle		**Micelle**		**Nanocapsule**					**Cellulose aggre-gates**
Inner material	H_2O	H_2O	Pluronic F127	PLA-PEG	HD	1-PHD	oleic acid	soy bean oil	BSA-dextran conjugate	cellulose
Shell material	Phospho-lipid mixtures	PiB-PEG-Me	Silica		PSAA	PMMA	Silica			
λ_{exc} / λ_{em} **(nm)**	532/400 630/450	630/450	532/430	532/430	514/450	633/550 708/555	635/470 635/505	635/525 635/550		850/595
Φ_{UC} **(%) at 20 °C**	2.3 0.3 – 2.4	0.2	2.2[a]	1.9[a]	N/A	N/A	3.3[b] 4.3[b]	1.7[b] 4.8[b]		N/A
I_{th} **(mW.cm^{-2})**	50 – 60	220 – 260	>360[a]	~100[a]	N/A	N/A	>>300[b]	50[b] 75[b]		N/A
Hydro-dynamic size (nm)	130 – 170	80 or 150	22	37	200	225	217	116 95		350
Reference	This thesis[21]	This thesis	[12a, 20b]	[33]	[20d]	[20a]	[12c]	[12b]		[20c]

[a] Influence of oxygen not reported. [b] Values obtained in air. PLA-PEG = polylactic acid-polyethylene glycol block copolymer, HD = hexadecane, 1-PHD = 1-phenylhexadecane, PiB-PEG-Me = polyisobutylene-polyethylene glycol block copolymer, PSAA = polystyrene-polyacrylic acid copolymer, PMMA = polymethyl methacrylate, BSA = bovine serum albumin

2.6 Thesis goal and outline

In the research described in this thesis, the goal was to prepare an upconverting nano-device that is able to generate blue light inside living cancer cells with which a light-sensitive ruthenium anticancer prodrug can be activated in order to kill the cells. The device should only become toxic upon light irradiation in the phototherapeutic window. To achieve this goal, it is likely that the following requirements need to be met:

i. high upconversion efficiency (Φ_{UC}) at human body temperature (37 °C)
ii. upconversion at low excitation intensity (*i.e.* a low I_{th}) so that use of high power lasers is prevented
iii. a large upconversion energy gain (ΔE_{UC}) to shift the activation wavelength to the phototherapeutic window (preferably red to near-infrared light)
iv. efficient energy transfer to the ruthenium prodrug
v. low oxygen sensitivity
vi. high temporal emission stability
vii. low cytotoxicity of the nano-device in the dark
viii. high cytotoxicity of the nano-device upon red to near-infrared light irradiation within a clinically relevant time span

In Chapter 3, I will describe how efficient red-to-blue and green-to-blue upconversion can be obtained in a liposome drug carrier. The red-to-blue upconversion is used to trigger the photodissociation of a ruthenium polypyridyl complex that is anchored to another liposome. In Chapter 4, the ruthenium complex is this time attached to the same liposome as that containing photosensitizer and annihilator molecules, and it is shown that the upconversion energy is transferred non-radiatively from the annihilator to the ruthenium complex *via* Förster resonance energy transfer (FRET). In Chapter 5 it is shown that red-to-blue upconversion is located in the lipid bilayer of the liposomes and that TTA-UC can be used to image the membrane of giant vesicles. Chapter 6 describes results of the investigation whether red-to-blue TTA-UC in liposomes is also efficient at human body temperature; I will describe how the upconversion efficiency is dependent on temperature in a variety of liposome compositions. Chapter 7 describes research that investigated whether a silica coating around the liposomes can protect the TTA-UC process from quenching by molecular oxygen. In Chapter 8 the *in vitro* applicability is addressed of liposomes that are functionalized with a red-to-

blue upconverting dye couple and ruthenium polypyridyl complexes, and whether it is possible to trigger a cytotoxic effect upon red light irradiation. Furthermore, the effect is of supplemental anti-oxidants on the performance of this system is reported. In Chapter 9 I will describe how red-to-blue upconversion can be obtained in polymersomes, and that the upconversion luminescence can be imaged in living cancer cells. Furthermore, I will address whether anti-oxidants increase the upconversion luminescence *in vitro*. Finally, in Chapter 10 the thesis is concluded by summing up the advantages and limits of TTA-UC for pro-drug activation, and future research directions are proposed.

2.7 References

[1] a) F. S. Mackay, J. A. Woods, H. Moseley, J. Ferguson, A. Dawson, S. Parsons, P. J. Sadler, *Chem. Eur. J.* **2006**, *12*, 3155-3161; b) A. F. Westendorf, J. A. Woods, K. Korpis, N. J. Farrer, L. Salassa, K. Robinson, V. Appleyard, K. Murray, R. Grünert, A. M. Thompson, P. J. Sadler, P. J. Bednarski, *Mol. Cancer Ther.* **2012**, *11*, 1894-1904; c) S. Perfahl, M. M. Natile, H. S. Mohamad, C. A. Helm, C. Schulzke, G. Natile, P. J. Bednarski, *Mol. Pharm.* **2016**.

[2] A. Y. Rwei, W. Wang, D. S. Kohane, *Nano Today* **2015**, *10*, 451-467.

[3] M. Schönberger, D. Trauner, *Angew. Chem., Int. Ed.* **2014**, *53*, 3264-3267.

[4] C. Ye, L. Zhou, X. Wang, Z. Liang, *Phys. Chem. Chem. Phys.* **2016**.

[5] M. Salierno, E. Marceca, D. S. Peterka, R. Yuste, R. Etchenique, *J. Inorg. Biochem.* **2010**, *104*, 418-422.

[6] J. Dong, Z. Xun, Y. Zeng, T. Yu, Y. Han, J. Chen, Y.-Y. Li, G. Yang, Y. Li, *Chem. Eur. J.* **2013**, *19*, 7931-7936.

[7] a) V. Nikolenko, R. Yuste, L. Zayat, L. M. Baraldo, R. Etchenique, *Chem. Commun.* **2005**, 1752-1754; b) A. Monguzzi, R. Tubino, S. Hoseinkhani, M. Campione, F. Meinardi, *Phys. Chem. Chem. Phys.* **2012**, *14*, 4322-4332.

[8] a) D. K. Chatterjee, M. K. Gnanasammandhan, Y. Zhang, *Small* **2010**, *6*, 2781-2795; b) C. Li, J. Lin, *J. Mater. Chem.* **2010**, *20*, 6831-6847; c) J. Shen, L. Zhao, G. Han, *Adv. Drug Delivery Rev.* **2012**; d) D. K. Chatterjee, L. S. Fong, Y. Zhang, *Adv. Drug Delivery Rev.* **2008**, *60*, 1627-1637; e) M. Lin, Y. Zhao, S. Wang, M. Liu, Z. Duan, Y. Chen, F. Li, F. Xu, T. Lu, *Biotechnol. Adv.* **2012**, *30*, 1551-1561.

[9] a) P. Zhang, W. Steelant, M. Kumar, M. Scholfield, *J. Am. Chem. Soc.* **2007**, *129*, 4526-4527; b) C. Wang, H. Tao, L. Cheng, Z. Liu, *Biomaterials* **2011**, *32*, 6145-6154; c) E. Ruggiero, J. Hernandez-Gil, J. C. Mareque-Rivas, L. Salassa, *Chem. Commun.* **2015**; d) W. Lv, T. S. Yang, Q. Yu, Q. Zhao, K. Y. Zhang, H. Liang, S. J. Liu, F. Y. Li, W. Huang, *Adv. Sci.* **2015**, *2*, 1500107; e) S. S. Lucky, K. C. Soo, Y. Zhang, *Chem. Rev.* **2015**; f) J. Zhou, Q. Liu, W. Feng, Y. Sun, F. Li, *Chem. Rev.* **2014**, *115*, 395-465; g) J. Liu, Y. Liu, W. Bu, J. Bu, Y. Sun, J. Du, J. Shi, *J. Am. Chem. Soc.* **2014**, *136*, 9701-9709.

[10] J.-C. Boyer, F. C. J. M. van Veggel, *Nanoscale* **2010**, *2*, 1417-1419.

[11] Z. Chen, W. Sun, H.-J. Butt, S. Wu, *Chem. Eur. J.* **2015**, *21*, 9165-9170.

[12] a) Q. Liu, T. Yang, W. Feng, F. Li, *J. Am. Chem. Soc.* **2012**, *134*, 5390-5397; b) Q. Liu, B. Yin, T. Yang, Y. Yang, Z. Shen, P. Yao, F. Li, *J. Am. Chem. Soc.* **2013**, *135*, 5029-5037; c) O. S. Kwon, H. S. Song, J. Conde, H.-i. Kim, N. Artzi, J.-H. Kim, *ACS Nano* **2016**, *10*, 1512-1521.

[13] a) J.-H. Kim, J.-H. Kim, *ACS Photonics* **2015**, *2*, 633-638; b) S. Baluschev, V. Yakutkin, G. Wegner, T. Miteva, G. Nelles, A. Yasuda, S. Chernov, S. Aleshchenkov, A. Cheprakov,

Appl. Phys. Lett. **2007**, *90*, 181103-181103; c) P. Mahato, A. Monguzzi, N. Yanai, T. Yamada, N. Kimizuka, *Nat. Mater.* **2015**, *14*, 924-930.
[14] a) C. A. Parker, C. G. Hatchard, *Proc. Chem. Soc.* **1962**, 386; b) C. A. Parker, C. G. Hatchard, T. A. Joyce, *Nature* **1965**, *205*, 1282-1284.
[15] a) T. N. Singh-Rachford, F. N. Castellano, *Coord. Chem. Rev.* **2010**, *254*, 2560-2573; b) J. Zhao, S. Ji, H. Guo, *RSC Adv.* **2011**, *1*, 937-950.
[16] S. M. Borisov, C. Larndorfer, I. Klimant, *Adv. Funct. Mater.* **2012**, *22*, 4360-4368.
[17] a) M. Filatov, S. Ritz, I. Ilieva, V. Mailänder, K. Landfester, S. Baluschev, *SPIE Newsroom* **2014**, *DOI: 10.1117/2.1201403.005378*; b) K. R. Menon, S. Jose, G. K. Suraishkumar, *Biotechnol. J.* **2014**, *9*, 1547-1553.
[18] a) M. Majek, U. Faltermeier, B. Dick, R. Pérez-Ruiz, A. Jacobi von Wangelin, *Chem. Eur. J.* **2015**, *21*, 15496-15501; b) O. S. Kwon, J. H. Kim, J. K. Cho, J. H. Kim, *ACS Appl. Mater. Interfaces* **2015**, *7*, 318-325.
[19] a) A. Monguzzi, S. M. Borisov, J. Pedrini, I. Klimant, M. Salvalaggio, P. Biagini, F. Melchiorre, C. Lelii, F. Meinardi, *Adv. Funct. Mater.* **2015**, *25*, 5617-5624; b) A. Nattestad, C. Simpson, T. Clarke, R. W. MacQueen, Y. Y. Cheng, A. Trevitt, A. J. Mozer, P. Wagner, T. W. Schmidt, *Phys. Chem. Chem. Phys.* **2015**; c) S. P. Hill, T. Banerjee, T. Dilbeck, K. Hanson, *J. Phys. Chem. Lett.* **2015**, *6*, 4510-4517; d) A. Nattestad, Y. Y. Cheng, R. W. MacQueen, T. F. Schulze, F. W. Thompson, A. J. Mozer, B. Fückel, T. Khoury, M. J. Crossley, K. Lips, G. G. Wallace, T. W. Schmidt, *J. Phys. Chem. Lett.* **2013**, *4*, 2073-2078.
[20] a) C. Wohnhaas, V. Mailänder, M. Dröge, M. A. Filatov, D. Busko, Y. Avlasevich, S. Baluschev, T. Miteva, K. Landfester, A. Turshatov, *Macromol. Biosci.* **2013**, *13*, 1422–1430; b) Q. Liu, W. Feng, T. Yang, T. Yi, F. Li, *Nat. Protocols* **2013**, *8*, 2033-2044; c) A. Nagai, J. B. Miller, P. Kos, S. Elkassih, H. Xiong, D. J. Siegwart, *ACS Biomater. Sci. Eng.* **2015**, *1*, 1206-1210; d) C. Wohnhaas, A. Turshatov, V. Mailänder, S. Lorenz, S. Baluschev, T. Miteva, K. Landfester, *Macromol. Biosci.* **2011**, *11*, 772-778.
[21] a) S. H. C. Askes, M. Kloz, G. Bruylants, J. T. Kennis, S. Bonnet, *Phys. Chem. Chem. Phys.* **2015**, *17*, 27380-27390; b) S. H. C. Askes, A. Bahreman, S. Bonnet, *Angew. Chem., Int. Ed.* **2014**, *53*, 1029-1033.
[22] T. W. Schmidt, F. N. Castellano, *J. Phys. Chem. Lett.* **2014**, *5*, 4062-4072.
[23] Y. C. Simon, C. Weder, *J. Mater. Chem.* **2012**, *22*, 20817-20830.
[24] T. N. Singh-Rachford, J. Lott, C. Weder, F. N. Castellano, *J. Am. Chem. Soc.* **2009**, *131*, 12007-12014.
[25] Y. Y. Cheng, B. Fückel, T. Khoury, R. l. G. C. R. Clady, N. J. Ekins-Daukes, M. J. Crossley, T. W. Schmidt, *J. Phys. Chem. A* **2011**, *115*, 1047-1053.
[26] a) Y. Y. Cheng, B. Fückel, T. Khoury, R. l. G. C. R. Clady, M. J. Y. Tayebjee, N. J. Ekins-Daukes, M. J. Crossley, T. W. Schmidt, *J. Phys. Chem. Lett.* **2010**, *1*, 1795-1799; b) Y. Y. Cheng, T. Khoury, R. G. C. R. Clady, M. J. Y. Tayebjee, N. J. Ekins-Daukes, M. J. Crossley, T. W. Schmidt, *Phys. Chem. Chem. Phys.* **2010**, *12*, 66-71; c) A. Haefele, J. Blumhoff, R. S. Khnayzer, F. N. Castellano, *J. Phys. Chem. Lett.* **2012**, *3*, 299-303.
[27] C. A. Parker, T. A. Joyce, *Chem. Commun.* **1966**, 108b-109.
[28] P. Mahato, N. Yanai, M. Sindoro, S. Granick, N. Kimizuka, *J. Am. Chem. Soc.* **2016**.
[29] P. Duan, N. Yanai, N. Kimizuka, *J. Am. Chem. Soc.* **2013**, *135*, 19056–19059.
[30] W. Wu, J. Sun, S. Ji, W. Wu, J. Zhao, H. Guo, *Dalton Trans.* **2011**, *40*, 11550-11561.
[31] a) R. R. Islangulov, J. Lott, C. Weder, F. N. Castellano, *J. Am. Chem. Soc.* **2007**, *129*, 12652-12653; b) A. Monguzzi, R. Tubino, F. Meinardi, *J. Phys. Chem. A* **2009**, *113*, 1171-1174; c) P. B. Merkel, J. P. Dinnocenzo, *J. Lumin.* **2009**, *129*, 303-306; d) X. Cui, J. Zhao, Y. Zhou, J. Ma, Y. Zhao, *J. Am. Chem. Soc.* **2014**, *136*, 9256-9259; e) F. Marsico, A. Turshatov, R. Peköz, Y. Avlasevich, M. Wagner, K. Weber, D. Donadio, K. Landfester, S. Baluschev, F. R. Wurm, *J. Am. Chem. Soc.* **2014**; f) A. J. Tilley, B. E. Robotham, R. P. Steer, K. P. Ghiggino, *Chem. Phys. Lett*; g) X. Jiang, X. Guo, J. Peng, D. Zhao, Y. Ma, *ACS Appl. Mater. Interfaces* **2016**; h) S. H. Lee, J. R. Lott, Y. C. Simon, C. Weder, *J. Mater. Chem. C* **2013**, *1*, 5142-5148; i) S.-H. Lee, Á. Sonseca, R. Vadrucci, E. Giménez, E. J. Foster, Y.

Simon, *J. Inorg. Organomet. Polym. Mater.* **2014**, *24*, 898-903; j) S. H. Lee, D. C. Thévenaz, C. Weder, Y. C. Simon, *J. Polym. Sci., Part A: Polym. Chem.* **2015**, *53*, 1629-1639.

[32] a) R. Vadrucci, C. Weder, Y. C. Simon, *Mater. Horiz.* **2015**, *2*, 120-124; b) P. Duan, N. Yanai, H. Nagatomi, N. Kimizuka, *J. Am. Chem. Soc.* **2015**, *137*, 1887-1894; c) T. Ogawa, N. Yanai, A. Monguzzi, N. Kimizuka, *Sci. Rep.* **2015**, *5*, 10882; d) Y. Murakami, Y. Himuro, T. Ito, R. Morita, K. Niimi, N. Kiyoyanagi, *J. Phys. Chem. B* **2016**, *120*, 748-755; e) R. Vadrucci, C. Weder, Y. C. Simon, *J. Mater. Chem. C* **2014**, *2*, 2837-2841.

[33] a) Z. Huang, X. Li, M. Mahboub, K. Hanson, V. Nichols, H. Le, M. L. Tang, C. J. Bardeen, *Nano Lett.* **2015**, *15*, 5552-5557; b) J.-H. Kim, F. Deng, F. N. Castellano, J.-H. Kim, *ACS Photonics* **2014**, *1*, 382-388; c) Y. C. Simon, S. Bai, M. K. Sing, H. Dietsch, M. Achermann, C. Weder, *Macromol. Rapid Commun.* **2012**, *33*, 498-502; d) K. Tanaka, H. Okada, W. Ohashi, J.-H. Jeon, K. Inafuku, Y. Chujo, *Bioorg. Med. Chem.* **2013**, *21*, 2678-2681; e) A. Turshatov, D. Busko, S. Baluschev, T. Miteva, K. Landfester, *New J. Phys.* **2011**, *13*, 083035; f) J.-H. Kim, J.-H. Kim, *J. Am. Chem. Soc.* **2012**, *134*, 17478-17481; g) C. Ye, B. Wang, R. Hao, X. Wang, P. Ding, X. Tao, Z. Chen, Z. Liang, Y. Zhou, *J. Mater. Chem. C* **2014**, *2*, 8507-8514; h) X. Cao, B. Hu, R. Ding, P. Zhang, *Phys. Chem. Chem. Phys.* **2015**; i) M. Penconi, P. L. Gentili, G. Massaro, F. Elisei, F. Ortica, *Photochem. Photobiol. Sci.* **2014**, *13*, 48-61; j) W. Wang, Q. Liu, C. Zhan, A. Barhoumi, T. Yang, R. G. Wylie, P. A. Armstrong, D. S. Kohane, *Nano Lett.* **2015**, *15*, 6332-6338; k) S. Mutsamwira, E. W. Ainscough, A. C. Partridge, P. J. Derrick, V. V. Filichev, *J. Phys. Chem. B* **2015**, *119*, 14045-14052; l) Z. Huang, X. Li, B. D. Yip, J. M. Rubalcava, C. J. Bardeen, M. L. Tang, *Chem. Mater.* **2015**, *27*, 7503-7507; m) C. Zhang, J. Y. Zheng, Y. S. Zhao, J. Yao, *Chem. Commun.* **2010**, *46*, 4959-4961; n) S. P. Hill, T. Dilbeck, E. Baduell, K. Hanson, *ACS Energy Lett.* **2016**, 3-8; o) D. C. Thévenaz, S. H. Lee, F. Guignard, S. Balog, M. Lattuada, C. Weder, Y. C. Simon, *Macromol. Rapid Commun.* **2016**; p) M. Poznik, U. Faltermeier, B. Dick, B. Konig, *RSC Adv.* **2016**, *6*, 41947-41950.

[34] A. Turshatov, D. Busko, Y. Avlasevich, T. Miteva, K. Landfester, S. Baluschev, *Chem. Phys. Chem.* **2012**, *13*, 3112-3115.

[35] a) M. Penconi, F. Ortica, F. Elisei, P. L. Gentili, *J. Lumin.* **2012**; b) A. Monguzzi, R. Tubino, F. Meinardi, *Phys. Rev. B* **2008**, *77*, 155122.

[36] R. R. Islangulov, D. V. Kozlov, F. N. Castellano, *Chem. Commun.* **2005**, 3776-3778.

[37] S. Hisamitsu, N. Yanai, N. Kimizuka, *Angew. Chem. Int. Ed.* **2015**, *54*, 11550-11554.

[38] a) P. C. Boutin, K. P. Ghiggino, T. L. Kelly, R. P. Steer, *J. Phys. Chem. Lett.* **2013**, 4113-4118; b) M. Tzenka, Y. Vladimir, N. Gabriele, B. Stanislav, *New J. Phys.* **2008**, *10*, 103002.

[39] A. J. Svagan, D. Busko, Y. Avlasevich, G. Glasser, S. Baluschev, K. Landfester, *ACS Nano* **2014**, *8*, 8198-8207.

[40] C. Wohnhaas, K. Friedemann, D. Busko, K. Landfester, S. Baluschev, D. Crespy, A. Turshatov, *ACS Macro Lett.* **2013**, *2*, 446-450.

[41] a) H. J. Feldmann, M. Molls, P. Vaupel, *Strahlenther. Onkol.* **1999**, *175*, 1-9; b) P. Vaupel, F. Kallinowski, P. Okunieff, *Cancer Res.* **1989**, *49*, 6449-6465; c) E. E. Graves, M. Vilalta, I. K. Cecic, J. T. Erler, P. T. Tran, D. Felsher, L. Sayles, A. Sweet-Cordero, Q.-T. Le, A. J. Giaccia, *Clin. Cancer Res.* **2010**, *16*, 4843-4852.

[42] a) I. Brigger, C. Dubernet, P. Couvreur, *Adv. Drug Delivery Rev*; b) J. Nam, N. Won, J. Bang, H. Jin, J. Park, S. Jung, S. Jung, Y. Park, S. Kim, *Adv. Drug Delivery Rev.* **2012**; c) C. Sanchez-Cano, M. J. Hannon, *Dalton Trans.* **2009**, 10702-10711; d) S. Svenson, *Mol. Pharm.* **2013**; e) A. Bansal, Y. Zhang, *Acc. Chem. Res.* **2014**.

[43] a) J. Liu, W. Bu, L. Pan, J. Shi, *Angew. Chem., Int. Ed.* **2013**, *52*, 4375-4379; b) L. Zhao, J. Peng, Q. Huang, C. Li, M. Chen, Y. Sun, Q. Lin, L. Zhu, F. Li, *Adv. Funct. Mater.* **2014**, *24*, 363-371; c) S. Cui, D. Yin, Y. Chen, Y. Di, H. Chen, Y. Ma, S. Achilefu, Y. Gu, *ACS Nano* **2012**.